Semiconductor Science and Technology

PAPER

Mid-IR plasmonic compound with gallium oxide toplayer formed by GaSb oxidation in water

To cite this article: Mario Bomers *et al* 2018 *Semicond. Sci. Technol.* **33** 095009

IOP Publishing Semiconductor Science and Technology
Semicond. Sci. Technol. 33 (2018) 095009 (9pp) https://doi.org/10.1088/1361-6641/aad4bf

Mid-IR plasmonic compound with gallium oxide toplayer formed by GaSb oxidation in water

Mario Bomers[1,4], Davide Maria Di Paola[2], Laurent Cerutti[1], Thierry Michel[3], Richard Arinero[1], Eric Tournié[1], Amalia Patanè[2] and Thierry Taliercio[1,4]

[1] IES, Université de Montpellier, CNRS, Montpellier, France
[2] School of Physics and Astronomy, The University of Nottingham, Nottingham NG7 2RD, United Kingdom
[3] L2C, Université de Montpellier, CNRS, Montpellier, France

E-mail: mario.bomers@umontpellier.fr and thierry.taliercio@umontpellier.fr

Received 23 May 2018, revised 5 July 2018
Accepted for publication 20 July 2018
Published 3 August 2018

Abstract

The oxidation of GaSb in aqueous environments has gained interest by the advent of plasmonic antimonide-based compound semiconductors for molecular sensing applications. This work focuses on quantifying the GaSb–water reaction kinetics by studying a model compound system consisting of a 50 nm thick GaSb layer on a 1000 nm thick highly Si-doped epitaxial grown InAsSb layer. Tracing of phonon modes by Raman spectroscopy over 14 h of reaction time shows that within 4 h, the 50 nm of GaSb, opaque for visible light, transforms to a transparent material. Energy-dispersive x-ray spectroscopy shows that the reaction leads to antimony depletion and oxygen incorporation. The final product is a gallium oxide. The good conductivity of the highly Si-doped InAsSb and the absence of conduction states through the oxide are demonstrated by tunneling atomic force microscopy. Measuring the reflectivity of the compound layer structure from 0.3 to 20 μm and fitting of the data by the transfer-matrix method allows us to determine a refractive index value of 1.6 ± 0.1 for the gallium oxide formed in water. The investigated model system demonstrates that corrosion, i.e. antimony depletion and oxygen incorporation, transforms the narrow band gap material GaSb into a gallium oxide transparent in the range from 0.3 to 20 μm.

Keywords: GaSb oxidation, gallium oxide, corrosion, water, plasmonics, refractive index

(Some figures may appear in colour only in the online journal)

1. Introduction

Antimonide-based compound semiconductors are promising narrow band gap materials for fast and low power consuming electronics [1], for mid-IR opto-electronic applications [2], for waveguide and optical parametric oscillator fabrication [3, 4], for photovoltaics [5–7] and for plasmonic applications [8, 9]. Developing a more comprehensive understanding of GaSb-compounds in aqueous environments is particularly important for biosensing applications in the mid-infrared spectral range [10]. Actually, the slow, steady and selective oxidation of GaSb in water leads to an all-semiconductor mid-IR pedestal configuration consisting of highly doped InAsSb plasmonic resonators on top of GaSb pedestals embedded in an amorphous oxide layer [11]. During the GaSb oxidation in water the group V-element Sb is depleted. A similar preferential dissolution of the group V-element was reported for the III–V semiconductor GaAs in aqueous environments [12].

On the one hand, there is an interest in better understanding of the hydrolytic instability of GaSb; on the other hand the galliums oxide formed by the reaction in water is of interest as it can serve for divers applications, e.g. the

[4] Authors to whom any correspondence should be addressed.

preparation of gas sensors, catalysts, phosphors, and optoelectronic devices [13–15]. The gallium oxide (Ga_2O_3), known as gallia, is an important semiconductor with a wide band gap of 4.9 eV, which can serve as a high-conductivity material for transparent electrodes. Synthesis in aqueous solution leads to polymorph gallia [14], but the homoepitaxial growth by metal organic vapor phase epitaxy leads to single-phase thin films of β-Ga_2O_3, whichs can be Si-doped [16].

The literature on GaSb oxidation distinguishes between the few nanometer thin native GaSb oxide formed in air and the much thicker oxide layers formed by plasma-, temperature- or wet-chemical oxidation. The native GaSb oxide is due to a thermodynamic equilibrium of GaSb and air, which leads to the formation of Ga_2O_3 and Sb_2O_3 [17, 18]. In a long-time oxidation study, the stability of the thin native oxide layer (<4 nm) was demonstrated [19]. However, the further oxidation of GaSb and Sb_2O_3 gives rise to elemental Sb, which is responsible for high surface leakage current [20]. Sulfur passivation can reduce the surface leakage current [20] and improve device performance [21–23], but the prevention of surface re-oxidation might only last a short-time (<1 day) [24].

Further insight in the oxidation reaction mechanism at the semiconductor/oxygen interface was recently obtained by scanning tunneling microscopy measurements which exploited the controlled exposure of a clean GaSb surface to oxygen [25]. The research on the reaction mechanism at GaSb/solution interfaces is ongoing and a recent study has shown that the redox processes are relevant for modifying the surface's electronic structure of GaSb during the reaction with an aqueous sodium sulfide solution [26]. In the field of plasmonic applications, a recent work has also demonstrated that the native oxide of GaSb can be exploited for stable surface functionalization based on phosphonic acid chemistry [27].

Top-down technological processes depend on controlled and selective etching of antimonide-based compound semiconductors [28, 29]. As etching consists of oxidation and reduction, two recent studies investigate the role of H_2O_2 and H_2O as oxidizers for GaSb etching [30, 31]. Contrary to InAs and $InAs_{0.9}Sb_{0.1}$ which are chemically stable in water [32], GaSb oxidizes in aqueous environment. The GaSb oxide formed by immersion of GaSb for two hours in water contains still significant quantity of Sb_2O_3 which is thermally unstable and can lead to unwanted conduction channels [33]. The electro-chemical process of anodic oxidation accelerates the process of GaSb oxidation. Therefore oxide layers, several hundreds of nanometer thick, can be formed in few minutes [34]. Compared to anodic oxidation, the GaSb oxidation in water is not driven by an external electro-chemical potential, but by exothermic reactions of GaSb with water, as demonstrated by density functional theory [35]. Antimony oxides are soluble in water [36] and therefore lead to corrosion. Gallium oxides are non-soluble in pure water [37].

In this work, we study a model compound system consisting of a 50 nm thick GaSb layer epitaxially grown on a 1000 nm thick layer of highly Si-doped InAsSb. The reaction of the GaSb with water over a period of 14 h is investigated by Raman spectroscopy, energy-dispersive x-ray spectroscopy (EDS), conductive atomic force microscopy and reflectometry in the visible and infrared spectral range. Electro-optical parameters of GaSb and InAsSb, [38, 39], spectral ellipsometrically determined constants of GaSb [40] and its anodically grown oxide [41, 42], as well as the electro-optical constants of gallium oxides [43–45] and of antimony oxide [46, 47] allow us to assess the product of the GaSb oxidation in water. In particular, we report a refractive index of $n = 1.6 \pm 0.1$ for the oxide, which is closer to the reported value of $n = 1.68$ for GaO_x [44] than the value reported for anodically grown GaSb oxide ($n = 2.0$).

2. Materials and methods

Solid-source molecular beam epitaxy (MBE) was used to grow 50 nm of GaSb on top of a 1000 nm thick Si-doped $InAs_{0.9}Sb_{0.1}$ layer. These two layers were grown on top of a 300 nm non-doped GaSb buffer layer, after the commercial available Te-doped (001) GaSb substrate was thermally de-oxidized under high vacuum conditions in the MBE-chamber. A doping level of $5 \times 10^{19}\,cm^{-3}$ was determined for the $InAs_{0.9}Sb_{0.1}$ layer [48]. The highly-doped $InAs_{0.9}Sb_{0.1}$-layer acts as a stop layer for the chemical reaction of the GaSb toplayer in water and as a mid-IR mirror for wavelength above the plasma wavelength, which is 5.5 μm for this doping level. The grown wafer was cleaved into 8 smaller pieces and each sample was immersed for a different amount of time in beakers filled with distilled water purified by the Purelab Option-Q and with resistivity of 13.4 MΩ cm at 23 °C. After a specific reaction time, the samples were removed and blown dry by nitrogen gas. For characterizing the samples, micro-Raman spectroscopy (Renishaw inVia microscope) was performed with an ×50 objective, 532 nm excitation laser wavelength, 3.4 mW incident power and 1 s acquisition time. Raman peaks were fitted with Lorentzians using the Fityk software [49]. Scanning electron microscopy (Fei Inspect S-50) was used to trace changes in the chemical composition by working in the EDS mode with an incident electron-beam energy of 8.0 kV and a magnification of ×5000. Information on the surface topography and conductivity were obtained by tunneling atomic force microscopy (TUNA) with the Nano-Man AFM (Bruker) equipped with a metal coated tip (PPP-ContPt-50). The reflectivity of the sample was measured in the visible spectral range by the Sopra GES-5 ellipsometer for an incident angle of 60° and an aluminum mirror as reference to normalize the reflectivity. In the IR-spectral range the Vertex 70 Fourier-transform IR spectrometer (Bruker) was used to measure the reflectivity of the samples for an incident angle of 60° and with a gold mirror as reference to normalize the spectra.

3. Raman spectroscopy to trace material transition of GaSb in water

The MBE grown layer structure, subdivided into smaller samples and immersed for different time duration in water

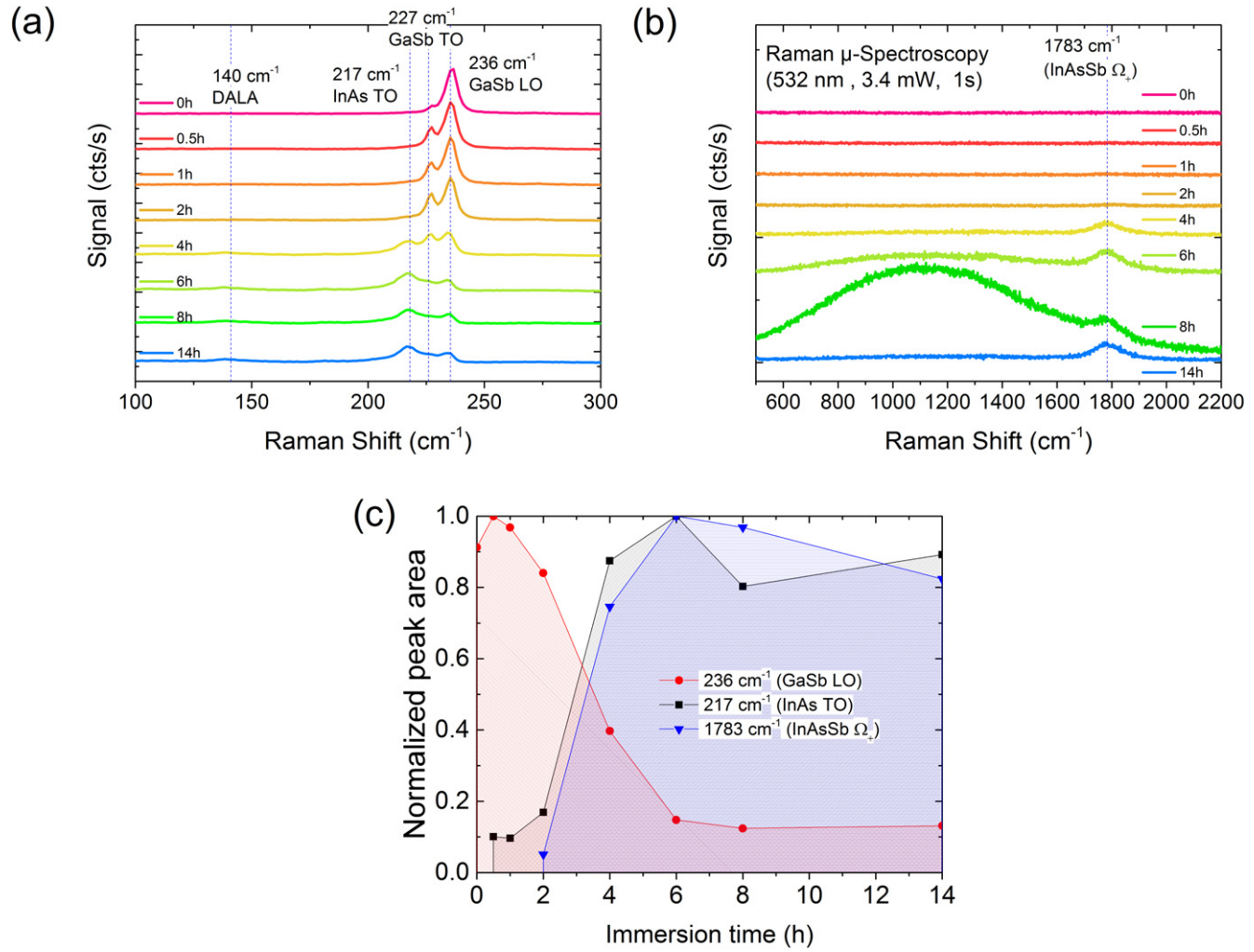

Figure 1. Raman spectroscopy performed with 532 nm excitation laser wavelength. (a) Measured phonon modes for GaSb/$InAs_{0.9}Sb_{0.1}$ compound system immersed for different amount of time to water (from 0 to 14 h). (b) Measured fluorescence and plasmon mode of the compound system. (c) Normalized peak area versus reaction time (immersion time) in water.

filled beakers, was investigated by Raman spectroscopy after drying by inert lab gas and storage at ambient conditions. In figure 1, the results of the Raman spectroscopy measurements are shown. The spectral region with significant phonon modes is shown in (a) and the spectral range with a plasmonic mode and fluorescence is shown in (b). The spectra were vertically shifted to clarify the identification of spectral features. In particular, in figure 1(a) clear changes of the active phonon modes can be seen. For the samples not immersed in water (0 h) or immersed for less than 4 h in water, the most dominant Raman shift are observable at 236 cm^{-1} and at 227 cm^{-1}. These peaks nearly disappear in between 6 h to 8 h of immersion and additional peaks appear. After 6 h of reaction with water, spectral signatures at 140 cm^{-1} and at 217 cm^{-1} can be identified. In figure 1(b), a spectral signature at 1783 cm^{-1} appears after 4 h of reaction with water. A broad signature, centered around 1100 cm^{-1}, can be observed after 6 h, then most strongly after 8 h, but finally it vanishes again after 14 h. We attribute this broad signature to fluorescence originating from Sb-oxide states [47]. The photon energy of the fluorescence is near 2.2 eV.

Table 1. Phonon frequencies of binary constituents of the layer structure and the plasmon frequencies of the highly Si-doped InAsSb.

Compound	Mode	Shift (cm^{-1})	Mode	Shift (cm^{-1})
InAs [39]	TO	217.3	LO	238.8
GaSb [39]	TO	227.0	LO	236.0
InAsSb:Si	Ω_-	217.0	Ω_+	1783.0

A literature comparison allows to assign the measured Raman peaks to phonon modes of binary constituents of the layer structure (see table 1). The phonon peaks that are decreasing with reaction time are attributed to GaSb and those appearing with reaction time to InAsSb. The signature at 140 cm^{-1} is attributed to a disorder-activated longitudinal acoustic phonon of the InAsSb-layer [39]. The peak at 1783 cm^{-1} is attributed to a phonon–plasmon coupled mode Ω_+ where the plasmon is due to the Si-doping of the InAsSb layer [50]. In the limit of wavevector $k \approx 0$, the frequencies

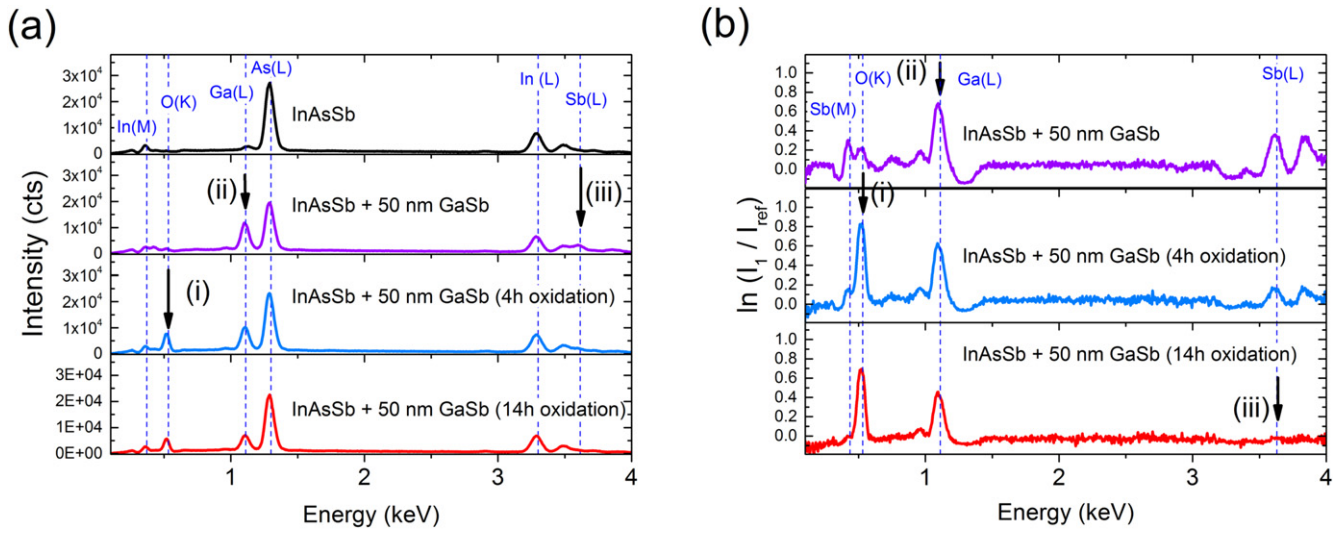

Figure 2. (a) Energy-dispersive x-ray spectra (EDS) of an InAsSb-layer without GaSb toplayer and of the compound system with GaSb toplayer are shown. The samples with toplayer were immersed for different time duration in water. (b) The spectra of the samples with toplayer are normalized to the reference spectra of an InAsSb-layer without toplayer to reveal changes in composition. The natural logarithm was taken to increase the contrast.

for the phonon–plasmon modes are given by [51]

$$\Omega_{\pm}^2 = \frac{1}{2}[(\omega_p^2 + \omega_{LO}^2) \pm \sqrt{(\omega_p^2 + \omega_{LO}^2)^2 - 4\omega_p^2\omega_{TO}^2}], \quad (1)$$

where ω_p is the plasma frequency, ω_{LO} the LO phonon frequency and ω_{TO} the TO phonon frequency of the InAsSb-layer. As $\omega_p \gg (\omega_{LO}, \omega_{TO})$ we find that $\Omega_- \approx \omega_{TO}$ and $\Omega_+ \approx \omega_p$. The found value of $\Omega_+ \approx \omega_p = 1783\,\mathrm{cm}^{-1}$ is in good agreement with the value of $\omega_p = 1818\,\mathrm{cm}^{-1}$ obtained by the Brewster angle method used to determine the plasma wavelength of the wafer [48].

The peak area for the signatures at Raman shifts of $236\,\mathrm{cm}^{-1}$, at $217\,\mathrm{cm}^{-1}$ and at $1783\,\mathrm{cm}^{-1}$ were determined for all eight samples. In figure 1(c), the evolution of the normalized peak area ratio is plotted versus the immersion time in water. It can be seen that the peak intensities attributed to GaSb decrease with immersion time and the modes attributed to InAsSb:Si increase with time. The intensity increase of the InAsSb modes is correlated with the disappearance of the GaSb modes. The immersion in water seems to transform the crystalline GaSb which absorbs strongly visible light (band gap at 0.72 eV) into a material transparent at 532 nm, thus the InAsSb:Si modes are no longer shielded by the 50 nm GaSb toplayer. After 6 h the GaSb peaks reaches a plateau, which indicates that the material transformation is complete and the material is no longer crystalline GaSb, but composed of antimony and gallium oxides.

4. SEM and EDS measurements

Changes in the chemical composition of the 50 nm GaSb-toplayer were investigated by EDS. Three samples, immersed for different time duration in water, were chosen for the investigation. Additionally, a reference sample consisting of 1 μm InAsSb:Si without 50 nm toplayer was characterized.

In figure 2(a) the measured EDS spectra are shown. The spectrum of the reference sample, consisting of 1 μm of InAsSb:Si epitaxially grown on GaSb, is shown on top. Below, the spectra of the samples with GaSb toplayer and with different time of immersion in water are shown (without immersion, 4 h of immersion and 14 h of immersion). Changes in chemical composition are indicated by black arrows. To focus on changes in chemical composition of the 50 nm thin toplayer, the spectra of the samples with 50 nm thick toplayer were normalized to the InAsSb:Si reference spectra without GaSb toplayer. Furthermore, the natural logarithm of this ratio was taken to increase the contrast. The result of the data treatment is shown in figure 2(b). The microscopes XPS-database allows to attribute the peaks to core-electron transitions. The spectral signature at 0.52 keV (i) can be assigned to the O(K) transition. Energetically close is the Sb(M) transition at 0.43 keV. Higher in energy are the Ga(L) line at 1.1 keV (ii) and the Sb(L) transition at 3.6 keV (iii). As the data treatment is optimized to reveal changes originating from the 50 nm toplayer, we clearly see in figure 2(a) that the main elements found for the GaSb toplayer not immersed in water are antimony and gallium with a small amount of oxygen. Immersion to water leads to a strong decrease of the antimony peaks and a strong increase of the oxygen peak. While after 4 h of reaction, some residues of Sb are part of the toplayer, these residues have vanished after 14 h. The observed changes in chemical composition are in good agreement with the Raman results concerning the hypothesis of fluorescence originating from Sb-oxides, which vanish after 14 h of reaction time.

We conclude that the immersion of the 50 nm GaSb toplayer in water has two major consequences in terms of modifying the material: (1) an incorporation of oxygen and (2) a depletion of antimony, which can be controlled by the time of immersion in water.

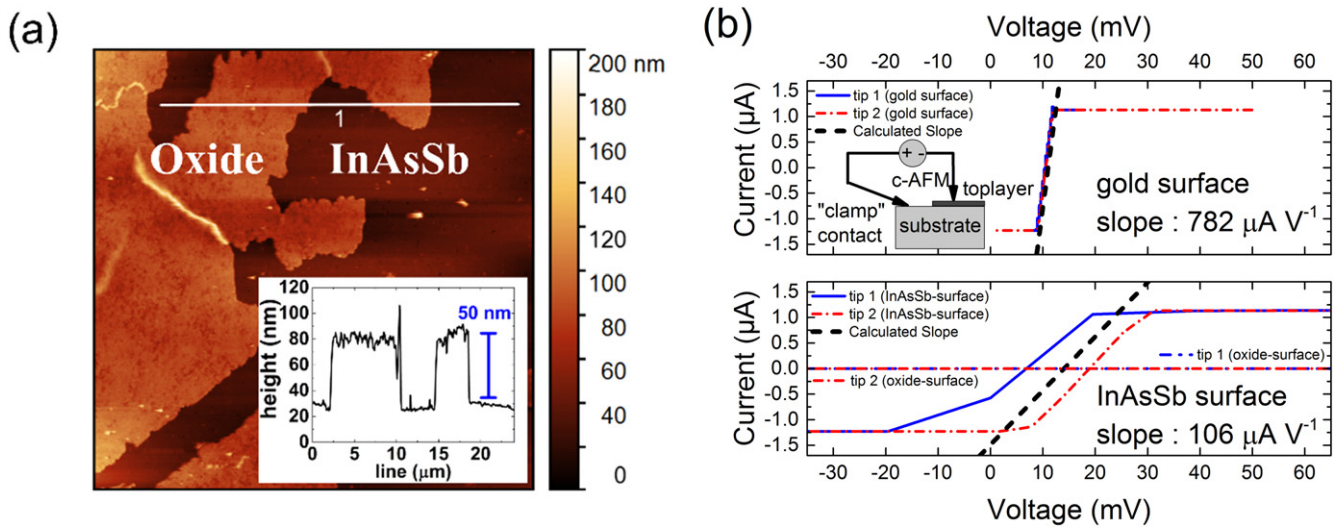

Figure 3. (a) Atomic force microscopy of the interface of the oxide and uncovered InAsSb surface. Inset: height profile acquired along line 1 in the main figure. (b) Tunneling atomic force microscopy (TUNA) on the gold reference sample and on the GaSb/InAsSb compound structure. Inset: sketch of the electric circuit formed by clamp contact and AFM-tip.

5. Tunneling atomic force microscopy (TUNA)

To further investigate the topological and electrical properties of the gallium oxide layer, we applied TUNA to the sample immersed for 14 h in water. By exposing half of the oxidized sample for 10 s to HCl:H_2O (1:5), the oxide in contact with the etching solution was removed and the underlying InAsSb:Si was uncovered. The other half of the surface, not exposed to the acidic solution, was unchanged. The uncovered InAsSb:Si surface was then contacted by a gold clamp and atomic force microscopy measurements were conducted at the interface between the etched and the non-etched region. Figure 3(a) shows the topography and the thickness of the oxide film measured at this interface. We determine a thickness of 55 nm ± 5 nm. Thus we conclude that the oxidation process does not significantly modify the thickness of the former crystalline 50 nm thick GaSb toplayer. By positioning the conductive tip either on the oxide or on the InAsSb-surface, we could measure the electric current versus the applied voltage by the electric circuit formed by the gold clamp, the InAsSb-surface and the tip. For the sake of illustration a sketch is added to the inset of figure 3(b). To obtain a reference current–voltage *I–V* curve, we used a gold surface with the same clamp system and the same tip. To obtain the highest current variation, the AFM tip was brought to contact with the surface such that ideally an ohmic contact is formed. The electronics of the TUNA microscope require to specify the detection range for low-current measurements. For the gold and the InAsSb-surface, a measurement range from −1.1 to 1.1 μA with current saturation outside of this range was chosen. On top of figure 3(b), *I–V* characteristics for the gold reference sample are plotted. The current increases linearly with voltage, thus a typical ohmic behavior can be observed. On the bottom of figure 3(b), the *I–V* results with the same tip and clamping system, but on the InAsSb-surface are represented. Subsequently, we measured again the gold surface to check for tip degradation and we repeated the experiment with a second tip. We find that the gold reference system has about seven times higher conductivity than the highly Si-doped InAsSb layer. We explain the lower conductivity of the Si-doped InAsSb layer by the native oxide of the InAsSb surface, which increases the tunneling distance by 1–3 nm, and by the 1000 times higher charge carrier density in gold.

Finally, we measured the current when the tip was positioned on the oxide and the clamp on the InAsSb:Si surface. A flat *I–V* curve was measured, i.e. no tunneling current was measured through the oxide layer. We repeated the experiment in the measurement range from −1.1 to 1.1 nA, but no current could be measured. This results demonstrates that the gallium oxide formed by immersion of non-doped GaSb in water is electrically insulating.

6. Reflectometry and fitting by transfer-matrix method

Our structure and the controlled thickness of the oxide layer are very suited for a reflectometry experiment with subsequent fitting by the transfer-matrix method to determine the optical properties of the Ga-oxide formed in water. To cover a wide spectral range, the VIS- and the IR-spectral ranges were measured with two different experimental setups (reflectivity normalized by an Al-mirror in the VIS-range and by a gold mirror in the IR-range). The result of this reflection measurement is shown in figure 4(a) for s- and for p-polarized light with an incident angle of 60°. It can be seen that the reflectance properties change with increasing immersion time. The strongest modification is observed for ultraviolet light from 300 to 400 nm for s-polarized light; a dip in reflection is observed after the sample was exposed for more than 4 h to water. In the IR-range, the modifications due to water immersion are perceptible as a shift of interference fringes. The onset of the highly reflective behavior is the plasma edge at 5.5 μm. While the Brewster mode [48], which is excited by

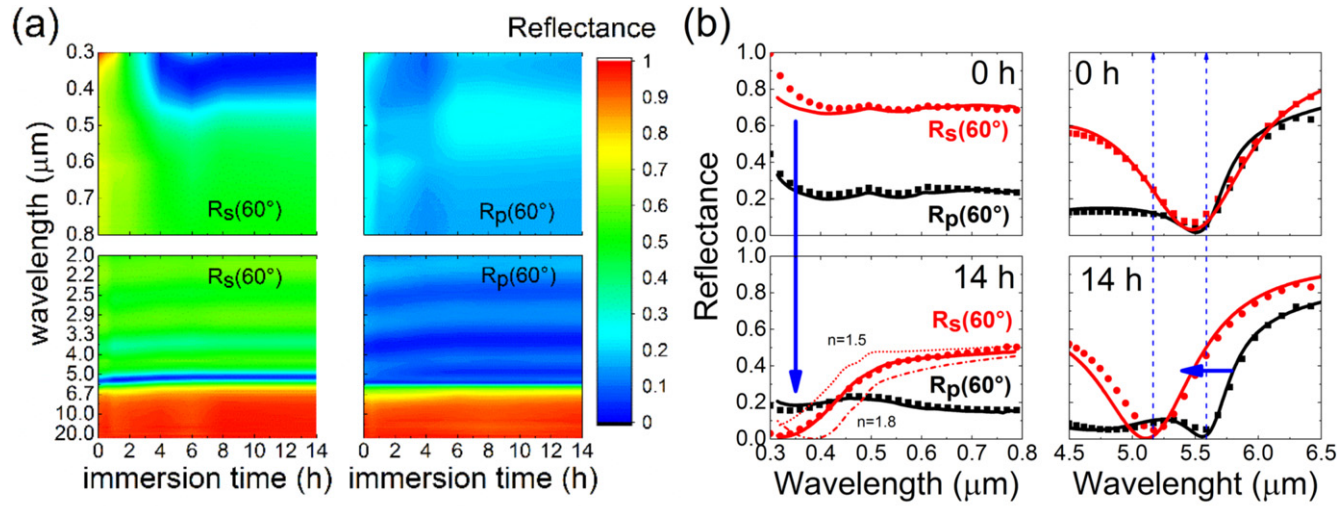

Figure 4. (a) Reflectance measurements in the visible and infrared spectral ranges for s- (left hand-side) and p-polarized (right hand-side) incident light with incidence angle of 60°. (b) Experimental data (points) and fitting curves (solid lines) for GaSb/InAsSb compound structure before (0 h) and after immersion to water (14 h). The dashed–dotted lines are fitting curves with different fitting values for the oxides refractive index n to illustrate an error interval for the best fit parameter.

p-polarized light, is nearly unaffected by the immersion process, the shift of a distinct dip in reflection is observed for s-polarized light in close proximity to the plasma edge.

The spectral regions where the reflectance was most affected by the immersion in water are shown in figure 4(b). The experimental data points were fitted by solid lines calculated by the transfer-matrix method [52]. We find a good agreement between the measurement and the fitting curves. As the transfer-matrix method requires geometrical and optical material properties to calculate the reflectance of a layer structure, we rely on tabulated values for GaSb and InAs in the visible range of light. We found that reported n, k-values for GaSb are suitable to model the material in the visible range (fit range from 300 to 800 nm), but in the infrared range (fit range from 2 to 20 μm) we rely on an analytical expression to describe the refractive index of GaSb [3]. The highly Si-doped InAsSb can be described by tabulated n, k-data of InAs in the visible spectral range. In the IR-range the semiconductor behaves like a metal due to the high doping. Therefore InAsSb can be described by the Drude-model in the IR-range [48]. Here, we report the value of $\omega_p = 1.05 \times 10^{15}\,\mathrm{rad\,s^{-1}}$, $\gamma_p = 1.3 \times 10^{13}\,\mathrm{rad\,s^{-1}}$ and $\varepsilon_\infty = 10.4$ as input parameter to the Drude equation to describe the IR-permittivity of InAsSb. The good agreement between the measured (black data points) and simulated reflectance (black line) in the visible range shows that the layer structure before immersion can be described by tabulated n, k-data (GaSb) for the 50 nm thick GaSb toplayer and tabulated n, k-data (InAs) for the InAsSb layer. This suggests that good material quality was obtained by MBE-growth. Fitting the measured reflectance in the infrared range allows to determine ω_p and γ_p describing the metallic behavior of InAsSb. The absorption losses in the residual doped GaSb wafer are accounted in the model by assuming the substrate to be semi-infinite. After 14 h of immersion the top-layer has become transparent to visible light as expected from Raman measurements. The obtained fit (red line) of the data (red data points) was obtained by assigning a value of $n = 1.6$ to the 50 nm thick oxide layer. In figure 4(b) the simulated curves for fit parameters of $n = 1.5$ and 1.8 (dashed–dotted lines) are added to demonstrate an error range for the fit value. The strongest sensitivity on the fit parameter is observed in the range from 300 to 400 nm. This can be explained in terms of an anti-reflective-coating effect of the oxide toplayer where the $\lambda/4$-criterion, $\lambda_0/(4 \cdot n)$, is fulfilled for an index of refraction of $n = 1.6 \pm 0.1$ (for incident light λ_0 of 300 nm and for a 50 nm toplayer). We conclude this part by comparing the found fit value for the gallium oxide formed from GaSb in water with similar materials in the spectral range from 0.3 to 20 μm. The found value of $n = 1.6 \pm 0.1$ is slightly lower than the reported values for anodically grown GaSb oxides ($n \approx 2.0$), but in good agreement with the refractive index value reported for Ga_2O_3 ($n = 1.68$) [44]. The higher refractive index of anodically formed GaSb oxide is probably due to the presences of antimony oxides, which are depleted by a slow corrosion process (several hours) when GaSb is immersed in water.

7. Discussion of results and proposed band structure

The measurements performed to characterize the oxidation of crystalline GaSb upon immersion in deionized water reveal that the oxidized layer is transparent to light in the visible, is mainly composed by gallium and oxygen, is non-conductive and has a comparable thickness as the reagent layer. Good fitting of its optical properties can be achieved by assuming a constant refractive index of $n = 1.6 \pm 0.1$ from 0.3 to 20 μm. We suggest water splitting, oxygen incorporation and antimony-dissolution as reaction mechanisms, which transforms GaSb into a gallium oxide when immersed in deionized

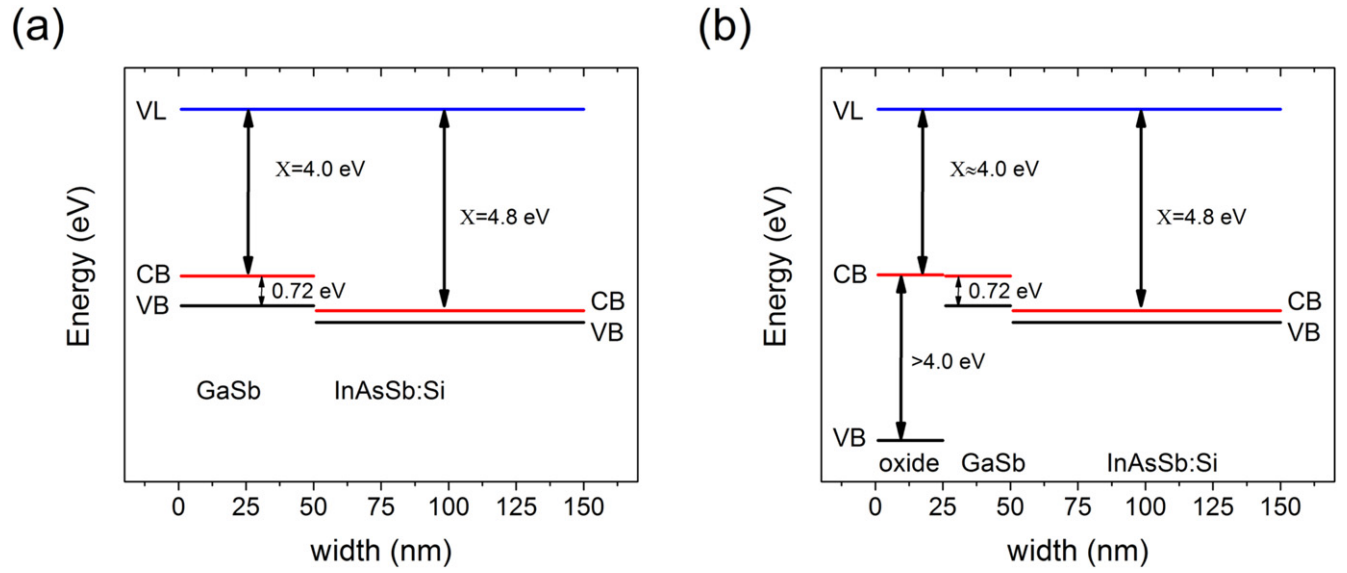

Figure 5. (a) Band alignment for GaSb/InAsSb heterostructure before immersion in water. (b) Proposed band structure to explain the transparency and the insulating behavior of 50 nm thick toplayer upon GaSb oxidation in water.

water. The end product of this reaction is a Ga-rich wide-band gap oxide.

While the band structure of crystalline $InAs_{1-x}Sb_x$/GaSb is well established, there exists a multitude of gallium and antimony oxides each with different crystal properties and band structures. *A priori*, we do not know if the material transition in deionized water leads to a known crystalline Ga-oxide configuration. Nevertheless, we can compare material properties derived from our study with those in the literature for Ga_2O_3 [44]. We find good agreement in terms of band gap (here >4.0 eV) and refractive index (here $n = 1.6 \pm 0.1$, compared to 1.68–1.74 for literature values). As the band offset between GaSb and InAsSb prevents the free-carriers in the highly Si-doped InAsSb ($\sim 5 \times 10^{19}$ cm^{-3}) to diffuse into the non-doped GaSb, a similar band offset seems plausible for the Ga-oxide. Assuming that the electron affinity X of the oxide formed in deionized water is close to the electron affinity of GaSb and β-Ga_2O_3 we summarize our findings in an energy band diagram. In figure 5(a), the out-of-equilibrium band alignment shows the GaSb/InAsSb before immersion in water. The changes in band gap due to the depletion of antimony and the incorporation of oxygen are shown in figure 5(b). The proposed energy band diagram explains the Raman measurement results, i.e. the appearance of InAsSb phonon modes upon immersion in water, and it explains the insulating behavior of the Ga-oxide toplayer.

8. Conclusion

We have shown that crystalline GaSb undergoes a material transition in water. The investigated model compound system of a 50 nm thick GaSb layer on a 1000 nm thick highly Si-doped InAsSb layer was grown by MBE. The InAsSb:Si serves as a chemical stop layer and a high conductive mid-IR plasmonic layer. We find that 50 nm of GaSb transforms within 14 h to Sb-depleted Ga-oxide. Already after 4 h of reaction time, the low-band gap material GaSb, opaque to visible light, transforms to a transparent material. Subsequently, the remaining antimony oxide continues to dissolve into solution such that the final product is a gallium oxide. The good conductivity of the highly Si-doped InAsSb and the absence of conduction states through the gallium oxide was demonstrated by TUNA. Measuring the reflectivity of the compound layer structure from 0.3 to 20 μm and fitting the data by the transfer-matrix method allowed to determine a refractive index value of 1.6 ± 0.1 for the oxide formed in water. The investigated model system demonstrates that corrosion, i.e. antimony depletion and oxygen incorporation, transforms the narrow band gap material GaSb into a gallium oxide transparent in the range from 0.3 to 20 μm. This study shows that the III–V semiconductor mid-IR plasmonic material platform based on GaSb can be combined with a gallium oxide surface.

Funding

French Investment for the Future program (EquipEx EXTRA, ANR 11-EQPX-0016); French ANR (SUPREME-B, ANR-14-CE26-0015); European Union's Horizon 2020 research and innovation programme (Marie Sklodowska-Curie grant agreement No 641899); Occitanie region.

Acknowledgments

J-M Peiris and J Lyonnet are acknowledged for technical support at the cleanroom facilities of the Université de Montpellier. G Boissier, J-M Aniel and G Narcy are acknowledged for technical support. Frederic Pichot is acknowledged for support and advices concerning the energy-

dispersive X-ray spectroscopy measurements. Michel Ramonda is acknowledged for support and advices regarding the tunneling atomic force microscopy measurements. Jean-Baptiste Rodriguez and Anthony Phimphachanh are acknowledged for discussion of the oxidation reaction mechanism.

ORCID iDs

Mario Bomers https://orcid.org/0000-0001-5481-8201
Richard Arinero https://orcid.org/0000-0002-2578-2606

References

[1] Bennett B R, Magno R, Boos J B, Kruppa W and Ancona M G 2005 Antimonide-based compound semiconductors for electronic devices: a review *Solid-State Electron.* **49** 1875–95
[2] Krier A (ed) 2006 *Mid-infrared Semiconductor Optoelectronics* (*Springer Series in Optical Sciences* vol 118) (Berlin: Springer)
[3] Roux S, Barritault P, Lartigue O, Cerutti L, Tournié E, Gérard B and Grisard A 2015 Mid-infrared characterization of refractive indices and propagation losses in GaSb/Al_XGa_{1-X}AsSb waveguides *Appl. Phys. Lett.* **107** 171901
[4] Roux S, Cerutti L, Tournie E, Gérard B, Patriarche G, Grisard A and Lallier E 2017 Low-loss orientation-patterned GaSb waveguides for mid-infrared parametric conversion *Opt. Mater. Express* **7** 3011
[5] Fraas L M, Avery J E, Martin J, Sundaram V S, Girard G, Dinh V T, Davenport T M, Yerkes J W and O'neil M J 1990 Over 35-percent efficient GaAs/GaSb tandem solar cells *IEEE Trans. Electron Devices* **37** 443–9
[6] Andreev V M, Sorokina S V, Timoshina N K, Khvostikov V P and Shvarts M Z 2009 Solar cells based on gallium antimonide *Semiconductors* **43** 668–71
[7] Lumb M P *et al* 2017 GaSb-based solar cells for full solar spectrum energy harvesting *Adv. Energy Mater.* **7** 1700345
[8] N'Tsame Guilengui V, Cerutti L, Rodriguez J-B, Tournié E and Taliercio T 2012 Localized surface plasmon resonances in highly doped semiconductors nanostructures *Appl. Phys. Lett.* **101** 161113
[9] Taliercio T, Ntsame Guilengui V, Cerutti L, Rodriguez J-B and Tournié E 2013 GaSb-based all-semiconductor mid-IR plasmonics *SPIE 8631, Quantum Sensing and Nanophotonic Devices X*863120
[10] Barho F B, Gonzalez-Posada F, Milla-Rodrigo M-J, Bomers M, Cerutti L and Taliercio T 2016 All-semiconductor plasmonic gratings for biosensing applications in the mid-infrared spectral range *Opt. Express* **24** 16175
[11] Bomers M, Barho F, Milla-Rodrigo M J, Cerutti L, Arinero R, Flores F G-P, Tournié E and Taliercio T 2018 Pedestal formation of all-semiconductor gratings through GaSb oxidation for mid-IR plasmonics *J. Phys. Appl. Phys.* **51** 015104
[12] Rei Vilar M, El Beghdadi J, Debontridder F, Artzi R, Naaman R, Ferraria A M and Botelho do Rego A M 2005 Characterization of wet-etched GaAs (100) surfaces *Surf. Interface Anal.* **37** 673–82
[13] Zhao Y, Frost R L, Yang J and Martens W N 2008 Size and morphology control of gallium oxide hydroxide GaO(OH), nano-to micro-sized particles by soft-chemistry route without surfactant *J. Phys. Chem.* C **112** 3568–79
[14] Li L, Wei W and Behrens M 2012 Synthesis and characterization of α-, β-, and γ-Ga_2O_3 prepared from aqueous solutions by controlled precipitation *Solid State Sci.* **14** 971–81
[15] Pearton S J, Yang J, Cary P H, Ren F, Kim J, Tadjer M J and Mastro M A 2018 A review of Ga_2O_3 materials, processing, and devices *Appl. Phys. Rev.* **5** 011301
[16] Gogova D, Wagner G, Baldini M, Schmidbauer M, Irmscher K, Schewski R, Galazka Z, Albrecht M and Fornari R 2014 Structural properties of Si-doped β-Ga_2O_3 layers grown by MOVPE *J. Cryst. Growth* **401** 665–9
[17] Schwartz G P 1983 Analysis of native oxide films and oxide-substrate reactions on III–V semiconductors using thermochemical phase diagrams *Thin Solid Films* **103** 3–16
[18] Wilmsen C W (ed) 1985 *Physics and Chemistry of III–V Compound Seimconductor Interfaces* (Boston, MA: Springer US) (https://doi.org/10.1007/978-1-4684-4835-1)
[19] Mizokawa Y, Komoda O and Miyase S 1988 Long-time air oxidation and oxide-substrate reactions on GaSb, GaAs and GaP at room temperature studied by x-ray photoelectron spectroscopy *Thin Solid Films* **156** 127–43
[20] Lin C L, Su Y K, Se T S and Li W L 1998 Variety transformation of compound at GaSb surface under sulfur passivation *Japan. J. Appl. Phys.* **37** L1543
[21] Lebedev M V, Kunitsyna E V, Calvet W, Mayer T and Jaegermann W 2013 Sulfur passivation of GaSb(100) surfaces: comparison of aqueous and alcoholic sulfide solutions using synchrotron radiation photoemission spectroscopy *J. Phys. Chem.* C **117** 15996–6004
[22] Tao D, Cheng Y, Liu J, Su J, Liu T, Yang F, Wang F, Cao K, Dong Z and Zhao Y 2015 Improved surface and electrical properties of passivated GaSb with less alkaline sulfide solution *Mater. Sci. Semicond. Process.* **40** 685–9
[23] Henry N C, Brown A, Knorr D B, Baril N, Nallon E, Lenhart J L, Tidrow M and Bandara S 2016 Surface conductivity of InAs/GaSb superlattice infrared detectors treated with thiolated self assembled monolayers *Appl. Phys. Lett.* **108** 011606
[24] Stine R, Aifer E H, Whitman L J and Petrovykh D Y 2009 Passivation of GaSb and InAs by pH-activated thioacetamide *Appl. Surf. Sci.* **255** 7121–5
[25] Mäkelä J, Tuominen M, Yasir M, Kuzmin M, Dahl J, Punkkinen M P J, Laukkanen P, Kokko K and Wallace R M 2015 Oxidation of GaSb(100) and its control studied by scanning tunneling microscopy and spectroscopy *Appl. Phys. Lett.* **107** 061601
[26] Lebedev M V, Lvova T V and Sedova I V 2018 Coordination of the chemical and electronic processes in GaSb(100) surface modification with aqueous sodium sulfide solution *J. Mater. Chem.* C **6** 5760–8
[27] Bomers M, Mezy A, Cerutti L, Barho F, Gonzalez-Posada Flores F, Tournié E and Taliercio T 2018 Phosphonate monolayers on InAsSb and GaSb surfaces for mid-IR plasmonics *Appl. Surf. Sci.* **451** 241–9
[28] Dier O, Lin C, Grau M and Amann M-C 2004 Selective and non-selective wet-chemical etchants for GaSb-based materials *Semicond. Sci. Technol.* **19** 1250–3
[29] Papis-Polakowska E 2005 Surface treatment of GaSb and related materials for the processing of mid-infrared semiconductor devices *Electron Technol. Internet J.* **37** 1–34
[30] Seo D, Na J, Lee S and Lim S 2015 Behavior of a GaSb (100) surface in the presence of H_2O_2 in wet-etching solutions *J. Phys. Chem.* C **119** 24774–80
[31] Seo D, Na J, Lee S and Lim S 2017 Behavior of GaSb (100) and InSb (100) surfaces in the presence of H_2O_2 in acidic and basic cleaning solutions *Appl. Surf. Sci.* **399** 523–34

[32] Jewett S A, Yoder J A and Ivanisevic A 2012 Surface modifications on InAs decrease indium and arsenic leaching under physiological conditions *Appl. Surf. Sci.* **261** 842–50
[33] Tsunoda K, Matsukura Y, Suzuki R and Aoki M 2016 *Thermal Instability of GaSb Surface Oxide Proceedings Volume 9819, Infrared Technology and Applications XLII* ed B F Andresen, G F Fulop, C M Hanson, J L Miller and P R Norton p 98190S
[34] Sulima O V, Bett A W and Wagner J 2000 Anodic oxidation of GaSb in acid-glycol-water electrolytes *J. Electrochem. Soc.* **147** 1910–4
[35] Bermudez V M 2013 First-principles study of the interaction of H_2O with the GaSb (001) surface *J. Appl. Phys.* **113** 184906
[36] Pitman A L, Pourbaix M and de Zoubov N 1957 Potential-pH diagram of the antimony–water system *J. Electrochem. Soc.* **104** 594
[37] Wills L A, Qu X, Chang I-Y, Mustard T J L, Keszler D A, Persson K A and Cheong P H-Y 2017 Group additivity-Pourbaix diagrams advocate thermodynamically stable nanoscale clusters in aqueous environments *Nat. Commun.* **8** 15852
[38] Mao Y and Krier A 1994 Energy-Band offsets and electroluminescence in n-$InAs_{1-x}Sb_{1-x}$/N-GaSb heterojunctions grown by liquid phase epitaxy *J. Electron. Mater.* **23** 503–7
[39] Cheetham K J, Carrington P J, Krier A, Patel I I and Martin F L 2012 Raman spectroscopy of pentanary GaInAsSbP narrow gap alloys lattice matched to InAs and GaSb *Semicond. Sci. Technol.* **27** 015004
[40] Muñoz M, Wei K, Pollak F H, Freeouf J L and Charache G W 1999 Spectral ellipsometry of GaSb: experiment and modeling *Phys. Rev.* B **60** 8105–10
[41] Aspnes D E, Schwartz B, Studna A A, Derick L and Koszi L A 1977 Optical properties of anodically grown native oxides on some Ga-V compounds from 1.5 to 6.0 eV *J. Appl. Phys.* **48** 3510
[42] Zollner S 1993 Model dielectric functions for native oxides on compound semiconductors *Appl. Phys. Lett.* **63** 2523–4
[43] Gowtham S, Deshpande M, Costales A and Pandey R 2005 Structural, energetic, electronic, bonding, and vibrational properties of Ga_3O, Ga_3O_2, Ga_3O_3, Ga_2O_3, and GaO_3 Clusters *J. Phys. Chem.* B **109** 14836–44
[44] He H, Orlando R, Blanco M A, Pandey R, Amzallag E, Baraille I and Rérat M 2006 First-principles study of the structural, electronic, and optical properties of Ga_2O_3 in its monoclinic and hexagonal phases *Phys. Rev.* B **74** 195123
[45] Mohamed M, Irmscher K, Janowitz C, Galazka Z, Manzke R and Fornari R 2012 Schottky barrier height of Au on the transparent semiconducting oxide β-Ga_2O_3 *Appl. Phys. Lett.* **101** 132106
[46] Tigau N, Ciupina V and Prodan G 2005 The effect of substrate temperature on the optical properties of polycrystalline Sb_2O_3 thin films *J. Cryst. Growth* **277** 529–35
[47] Allen J P, Carey J J, Walsh A, Scanlon D O and Watson G W 2013 Electronic structures of antimony oxides *J. Phys. Chem.* C **117** 14759–69
[48] Taliercio T, Guilengui V N, Cerutti L, Tournié E and Greffet J-J 2014 Brewster 'mode' in highly doped semiconductor layers: an all-optical technique to monitor doping concentration *Opt. Express* **22** 24294
[49] Wojdyr M 2010 *Fityk* : a general-purpose peak fitting program *J. Appl. Crystallogr.* **43** 1126–8
[50] Di Paola D M *et al* 2018 Optical detection and spatial modulation of mid-infrared surface plasmon polaritons in a highly doped semiconductor *Adv. Opt. Mater.* **6** 1700492
[51] Palik E D and Furdyna J K 1970 Infrared and microwave magnetoplasma effects in semiconductors *Rep. Prog. Phys.* **33** 1193–322
[52] Born M and Wolf E 1970 *Principles of Optics* (Oxford: Pergamon)